Beyond-mean-field description of octupolarity in dysprosium isotopes with the Gogny-D1M energy density functional

R. Rodríguez-Guzmán[1,*] and L. M. Robledo[2,3,†]

[1]*Departamento de Física Aplicada I, Escuela Politécnica Superior, Universidad de Sevilla, 41011 Seville, Spain*

[2]*Center for Computational Simulation, Universidad Politécnica de Madrid, Campus Montegancedo, 28660 Boadilla del Monte, Madrid, Spain*

[3]*Departamento de Física Teórica and CIAFF, Universidad Autónoma de Madrid, 28049 Madrid, Spain*

(Received 16 May 2023; revised 14 June 2023; accepted 21 July 2023; published 7 August 2023)

The emergence and stability of (static) octupole deformation effects in Dy isotopes from drip line to drip line ($72 \leqslant N \leqslant 142$) are analyzed in this paper using mean-field and beyond-mean-field techniques often used for this purpose. We find static octupole deformations at the Hartree-Fock-Bogoliubov (HFB) level with the Gogny-D1M force for $N \approx 134$ isotopes, while nuclei with $N \approx 88$ exhibit reflection-symmetric ground states. It is shown that, given the softness found in the mean-field and parity-projected potential energy surfaces along the octupole direction, neither of these two levels of approximation is sufficient to extract conclusions about the (permanent and/or vibrational) nature of octupole dynamic in Dy isotopes. From the analysis of the collective wave functions as well as the excitation energies of the first negative-parity states and $B(E3)$ strengths, obtained within the framework of a two-dimensional symmetry-conserving generator coordinate method (2D-GCM), it is concluded that the increased octupole collectivity in Dy isotopes with $N \approx 88$ and $N \approx 134$ is a vibrational-like effect that is not directly related to permanent mean-field octupole deformation in the considered nuclei. A pronounced suppression of the $B(E1)$ strengths is predicted for isotopes with $N \approx 82$ and $N \approx 126$. The comparison of results obtained with other parametrizations shows the robustness of the predicted trends with respect to the underlying Gogny energy density functional.

DOI: 10.1103/PhysRevC.108.024301

I. INTRODUCTION

The majority of the spherical and/or quadrupole-deformed nuclear ground states are reflection symmetric. However, due to the mean-field spontaneous symmetry breaking mechanism [1] reflection-asymmetric ground states tend to be favored energetically in certain regions of the nuclear chart [2]. Those regions are usually associated with the neutron/proton numbers $N/Z = 34$, 56, 88, and 134 where the coupling between intruder $(N+1, l+3, j+3)$ and normal-parity (N, l, j) states is more effective in developing octupole deformed ground states. Octupole-related features have been studied around the already mentioned neutron/proton numbers; however, the search for new islands of reflection-asymmetric shapes, all over the nuclear chart, still represents one of the frontiers in nuclear structure physics nowadays. Within this context, a better understanding of the permanent and/or vibrational nature of octupole dynamic in atomic nuclei still represents a major challenge that cannot be resolved with plain mean field calculations.

Octupolarity along the Dy isotopic chain has been the subject of experimental studies. For example, bands associated with parity doublets have been studied in ^{157}Dy using the JUROGAM II array [3]. A rotational band, built on an octupole vibration, has been identified in ^{152}Dy [4]. The $E1$ transitions between opposite parity bands have been studied in ^{154}Dy [5]. Negative parity bands have also been investigated in both ^{156}Dy and ^{162}Dy [6,7]. The experimental findings [3–7] raise questions about the impact of octupole correlations in the structural evolution along the Dy isotopic chain as well as on the (permanent and/or vibrational) nature of octupole deformation effects in those isotopes. Recently, relativistic mean-field calculations have been carried out for Dy nuclei [8]. On the basis of plain mean-field results, it has been concluded that $N \approx 88$ and $N \approx 134$ Dy isotopes exhibit permanent octupole deformation. The conclusion extends to isotopes where the octupole minima found in the calculations are very shallow and the corresponding potential energy surfaces exhibit a rather soft behavior along the octupole direction. The conclusions of Ref. [8] are at variance with previous macroscopic-microscopic (mac-mic) results [9] as well as with the ones extracted from this microscopic study, in which the relevance of beyond-mean-field octupole dynamics in Dy isotopes is considered with the Gogny energy density functional (EDF) [10], using the models already introduced in Refs. [11–14] and used to describe octupole dynamics in other regions of the nuclear chart. In particular, we address in the present study the stability of (static) mean-field octupole deformation effects once beyond-mean-field symmetry restoration and/or configuration mixing (dynamical) effects are taken into account. To this end, calculations have been

*raynerrobertorodriguez@gmail.com
†luis.robledo@uam.es

carried out along the Dy isotopic chain from proton to neutron drip line ($72 \leqslant N \leqslant 142$).

A lot of effort has been devoted to better understand basic fingerprints of octupole correlations (see, for example, Refs. [15–25] and references therein). Previous experiments have found evidence for octupole deformed ground states in ^{144,146}Ba [21,22] and ^{222,224}Ra [24,25]. The measured low-lying states in ^{224,226}Rn suggest that those isotopes should be characterized as octupole vibrations [26]. Furthermore, fingerprints of octupole correlations have also been found in the case of ^{228}Ra and ^{228}Th [24,27]. Here, one should keep in mind that renewed interest in octupole correlations also comes from the need to improve the description of fission paths in heavy and superheavy nuclei. In particular octupole correlations are well known to affect the outer sectors of the fission paths in those nuclei (see, for example, Refs. [28–31] and references therein). Octupole deformation is also one of the collective coordinates at play in the case of cluster radioactivity [32].

A wide range of models have been employed to study octupole dynamics. For example, octupole shapes have been considered within the mac-mic framework [9,33–37] as well as within the mapped interacting boson model (IBM) [38–45]. Octupole correlations have also been the subject of intense microscopic scrutiny, both at the mean-field level and beyond, using nonrelativistic and relativistic approximations [46–65].

In the case of the Gogny energy density functional (EDF) [10], the models of Refs. [11–14] have already been employed to study the quadrupole-octupole coupling in regions of the nuclear chart such as the Sm and Gd isotopes with $84 \leqslant N \leqslant 92$ [11], actinide nuclei with neutron number $N \approx 134$ [12], Rn, Ra, and Th isotopes [13], as well as neutron-rich actinides and superheavy nuclei [14]. First, the quadrupole Q_{20} and octupole Q_{30} deformation parameters have been considered simultaneously within the constrained Hartree-Fock-Bogoliubov (HFB) framework [1] to build the corresponding (Q_{20}, Q_{30}) mean-field potential energy surfaces (MFPESs). Second, the changes induced in the MFPESs by the restoration of the reflection symmetry have been considered by projecting the (Q_{20}, Q_{30})-constrained intrinsic HFB states onto a good parity. Third, the quadrupole-octupole coupling has been taken into account using a two-dimensional symmetry-conserving generator coordinate method (2D-GCM) ansatz [11–14].

The key lesson extracted from the studies mentioned above [11–14] is that, for the considered nuclei, 2D-GCM zero-point quantum fluctuations are essential to obtain a systematic of the $B(E1)$ and $B(E3)$ strengths as well as of the excitation energies of the lowest negative-parity states that accounts reasonably well for the available experimental data. Moreover, it has also been shown that such 2D-GCM quantum fluctuations can lead to an enhanced octupolarity as well as to a weaker dependence of the correlation energies with neutron number. In this respect, we also refer the reader to previous large scale surveys, using the octupole degree of freedom as a single generating coordinate [64,65].

The main aim of this paper is to address, the stability of mean-field octupole deformation effects as well as the impact of beyond-mean-field (dynamical) correlations in dripline-to-dripline calculations for Dy isotopes. Our results reexamine the conclusions of relativistic mean-field [8] studies around both $N = 88$ and $N = 134$ pointing to permanent octupole deformation effects in those regions. In order to disentangle the role of static octupole deformation, we first obtained a set of (Q_{20}, Q_{30})-constrained Gogny-HFB wave functions for the even-even isotopes $^{138-208}$Dy. The energies corresponding to each of these mean-field states are then used to build the MFPESs as functions of the quadrupole Q_{20} and octupole Q_{30} deformations. Note that the considered range of neutron numbers, i.e., $72 \leqslant N \leqslant 142$, includes the octupole magic number $N = 88$ and extends up to a very neutron-rich sector to also include the octupole magic number $N = 134$. Therefore, the Gogny-HFB calculations allow us to examine the emergence and evolution of static ground state reflection-asymmetric shapes along the Dy isotopic chain and, in particular, to compare with mac-mic [9] and relativistic mean-field [8] predictions around both $N = 88$ and $N = 134$.

As will be shown later on in the paper, for the studied isotopes, the MFPESs often are rather soft along the Q_{30} direction and/or the mean-field octupole correlation energies $E_{\mathrm{CORR,HFB}}$ [see Eq. (8)] are rather small. Moreover, in some cases the MFPESs exhibit a transitional behavior along the Q_{20} direction. Taking into account the experience obtained in previous works [11–14] on the role of dynamical correlations in such scenarios and the mean-field results already mentioned, we then studied the impact of beyond-mean-field zero-point quantum fluctuations in $^{138-208}$Dy. To this end, we have resorted to both parity symmetry restoration and symmetry-conserving 2D-GCM quadrupole-octupole configuration mixing [11–14].

The results discussed in this paper, at the three levels of approximation employed, have been obtained with the parametrization D1M [66] of the Gogny EDF. The parametrization D1M has already been shown to provide a reasonable description of octupole-related features in previous studies [11–14]. However, in some instances, we will also discuss results obtained with the parametrizations D1S [10] and D1M* [67] in order to illustrate the robustness of the predictions with respect to the underlying Gogny EDF.

The paper is organized as follows. The HFB and beyond-mean-field approximations employed in this study are briefly outlined in Secs. II A and II B. The results obtained with the corresponding approach will be discussed in each section. The HFB results will be discussed in Sec. II A, while dynamical beyond-mean-field correlations are considered in Sec. II B. In particular, parity symmetry restoration is considered in Sec. II B 1, while symmetry-conserving 2D-GCM quadrupole-octupole configuration mixing is discussed in Sec. II B 2. In this Sec. II B 2, the excitation energies of the lowest negative-parity states as well as $B(E1)$ and $B(E3)$ strengths obtained for $^{138-208}$Dy will be discussed and compared with the available experimental data [68]. Furthermore, we will also illustrate the robustness of the 2D-GCM predictions with respect to the underlying Gogny-EDF. Finally, Sec. III is devoted to the concluding remarks.

II. RESULTS

In this work we study the emergence and stability of octupole deformation effects in the isotopic chain $^{138-208}$Dy

from a microscopic point of view using the density-dependent Gogny-D1M EDF. To this end, the HFB approach [1], with constrains on the axially symmetry quadrupole $\hat{Q}_{20}$ and octupole $\hat{Q}_{30}$ operators, is employed as a first step. On the other hand dynamical beyond-mean-field correlations are considered via parity projection of the intrinsic HFB states and/or symmetry-conserving 2D-GCM quadrupole-octupole configuration mixing. In this section, we briefly outline these approaches [11–14] and discuss the results obtained with each of them.

A. Hartree-Fock-Bogoliubov

We first performed (Q_{20}, Q_{30})-constrained Gogny-D1M HFB calculations for $^{138–208}$Dy. In the calculations the HFB equation was solved with constraints on the axially symmetric quadrupole

$$\hat{Q}_{20} = \tfrac{1}{2}(x^2 + y^2) \tag{1}$$

and octupole

$$\hat{Q}_{30} = z^2 - \tfrac{3}{2}(x^2 + y^2)z \tag{2}$$

operators, using an approximate second-order gradient method [69]. A constraint on the operator $\hat{Q}_{10}$ was also used to fix the center of mass at the origin [11]. The HFB quasiparticle operators [1] were expanded in a (deformed) axially symmetric harmonic oscillator (HO) basis containing 15 major shells. Axial symmetry was kept as a self-consistent symmetry in order to alleviate the computational effort.

For each of the intrinsic states $|\Phi(Q_{20}, Q_{30})\rangle$ obtained in the constrained Gogny-HFB calculations, the quadrupole Q_{20} and octupole Q_{30} deformations are defined as the mean values

$$Q_{20} = \langle\Phi(Q_{20}, Q_{30})|\hat{Q}_{20}|\Phi(Q_{20}, Q_{30})\rangle \tag{3}$$

and

$$Q_{30} = \langle\Phi(Q_{20}, Q_{30})|\hat{Q}_{30}|\Phi(Q_{20}, Q_{30})\rangle. \tag{4}$$

The corresponding deformation parameters β_λ $(\lambda = 2, 3)$ are then defined as

$$\beta_\lambda = \frac{\sqrt{4\pi(2\lambda+1)}}{3R_0^\lambda A} Q_{\lambda 0} \tag{5}$$

with $R_0 = 1.2A^{1/3}$ and A the mass number. For example, for $A = 150$ a quadrupole deformation $Q_{20} = 5b$ is equivalent to $\beta_2 = 0.217$, whereas for $A = 200$ an octupole deformation $Q_{30} = 2.5b^{3/2}$ is equivalent to $\beta_3 = 0.113$.

The Gogny-HFB MFPESs are depicted in Fig. 1 for a selected set of Dy isotopes, as illustrative examples. Those MFPESs are nothing else than the HFB energies

$$E_{\rm HFB}(Q_{20}, Q_{30}) = \frac{\langle\Phi(Q_{20}, Q_{30})|\hat{H}|\Phi(Q_{20}, Q_{30})\rangle}{\langle\Phi(Q_{20}, Q_{30})|\Phi(Q_{20}, Q_{30})\rangle} \tag{6}$$

corresponding to each of the intrinsic states $|\Phi(Q_{20}, Q_{30})\rangle$. The HFB energies (6) are invariant under the exchange of Q_{30} into $-Q_{30}$ to be associated to the parity symmetry of the interaction,

$$E_{\rm HFB}(Q_{20}, Q_{30}) = E_{\rm HFB}(Q_{20}, -Q_{30}). \tag{7}$$

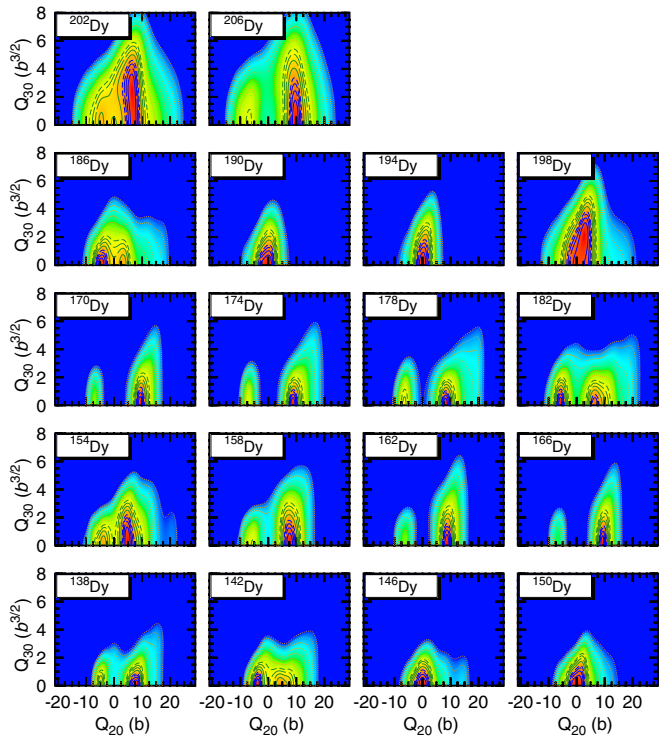

FIG. 1. MFPESs computed with the Gogny-D1M EDF for a selected set of Dy isotopes. Dark blue contour lines extend from 0.25 MeV up to 1 MeV above the ground state energy in steps of 0.25 MeV in the ascending sequence of full, long-dashed, medium-dashed, and short-dashed lines. Dark green contour lines extend from 1.5 MeV up to 3 MeV above the ground state in steps of 0.5 MeV with the same sequence of full, long-dashed, medium-dashed, and short-dashed lines as before. From there on, orange dotted contour lines are drawn in steps of 1 MeV. The color code spans a range of 10 MeV with red corresponding to the lowest energy and blue corresponding to an energy 10 MeV above. The intrinsic HFB energies are symmetric under the exchange $Q_{30} \to -Q_{30}$. For $A = 150$ a quadrupole deformation $Q_{20} = 5b$ is equivalent to $\beta_2 = 0.217$, whereas for $A = 200$ an octupole deformation $Q_{30} = 2.5\,b^{3/2}$ is equivalent to $\beta_3 = 0.113$. For more details, see the main text.

As a consequence of this invariance, only the energies corresponding to $Q_{30} \geqslant 0$ values are included in Fig. 1. In the calculations, the Q_{20} grid $-25b \leqslant Q_{20} \leqslant 35b$ (with a step $\delta Q_{20} = 1b$) and the Q_{30} grid $0b^{3/2} \leqslant Q_{30} \leqslant 10b^{3/2}$ (with a step $\delta Q_{30} = 0.25b^{3/2}$) were employed.

The ground state quadrupole deformations are plotted, as functions of the neutron number N, in panel (a) of Fig. 2 for $^{138–208}$Dy. The corresponding β_2 deformation parameters are depicted in panel (b) of the same figure. Along the Q_{20} direction there is a shape/phase transition from a prolate (^{138,140}Dy) to an oblate (^{142,144}Dy) ground state, followed by spherical ground states in $^{146–150}$Dy, reflecting the proximity to the neutron shell closure $N = 82$. With increasing neutron number, the ground state quadrupole deformations increase, reaching values of $Q_{20} = (8–9)b$ for $92 \leqslant N \leqslant 112$. This is, once more, followed by shape/phase transitions to oblate ground states in $^{182–188}$Dy and then to spherical ground states in $^{190–196}$Dy, associated with the proximity to the neutron shell

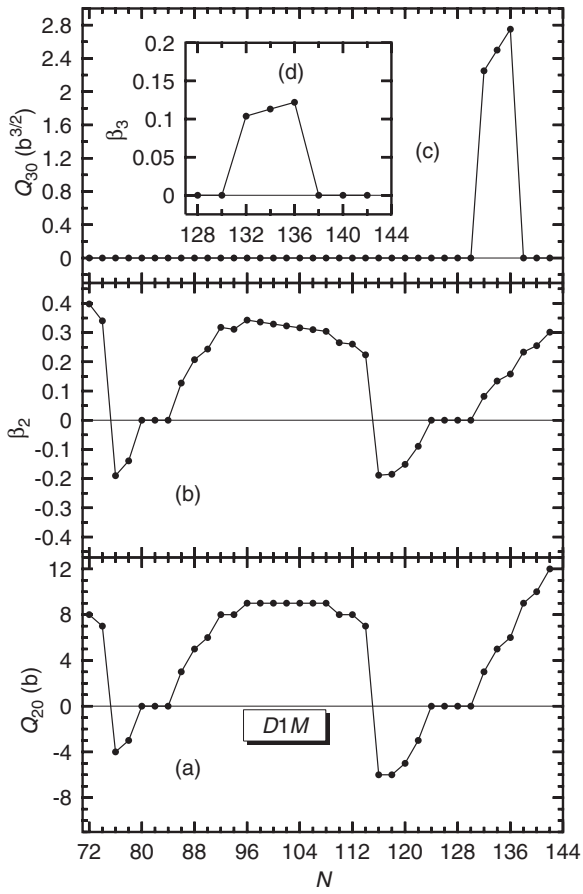

FIG. 2. The mean field ground state quadrupole (octupole) deformations are plotted, as functions of the neutron number N, in panel (a) [(c)] for $^{138-208}$Dy. The corresponding quadrupole (octupole) deformation parameters β_2 (β_3) are also depicted in panel (b) [(d)]. Results have been obtained with the Gogny-D1M EDF.

closure $N = 126$. For larger neutron numbers, the ground state quadrupole deformations exhibit a pronounced increase, reaching the value $Q_{20} = 12b$ for ^{208}Dy.

For the considered Dy isotopes, the ground state quadrupole deformations are within the range $-6b \leqslant Q_{20} \leqslant 12b$ ($-0.19 \leqslant \beta_2 \leqslant 0.34$). The results obtained with Gogny-D1M, as well as the ones obtained with the D1S and D1M* parametrizations, for the ground state quadrupole deformations agree well with previous mac-mic [9] and reflection-asymmetric relativistic mean-field [8] results. Note that, for some of the considered isotopes, the MFPESs depicted in Fig. 1 exhibit transitional features along the Q_{20} direction.

As can be seen from Fig. 1 and from panels (c) and (d) of Fig. 2, static Gogny-D1M ground state octupole deformations are only predicted for $^{198-202}$Dy, i.e., for very neutron-rich isotopes around $N = 134$. In this case, the ground state octupole deformations are within the range $2.25b^{3/2} \leqslant Q_{30} \leqslant 2.75b^{3/2}$ ($0.10 \leqslant \beta_3 \leqslant 0.12$). Octupole-deformed neutron-rich nuclei have already been predicted in this [8,9] and other regions of the nuclear chart [14,36,50,61–63]. The soft behavior of the Gogny-D1M MFPESs along the Q_{30} direction, as one approaches the neutron number $N = 134$, becomes apparent from Fig. 1. Nevertheless, even in the case of nuclei with octupole deformed mean-field ground states (i.e., $^{198-202}$Dy), the HFB energy gained by breaking reflection symmetry,

$$E_{\mathrm{CORR,HFB}} = E_{\mathrm{HFB},Q30=0} - E_{\mathrm{HFB,GS}}, \tag{8}$$

and defined as the difference between the HFB energy corresponding to the absolute minimum obtained in reflection-symmetric calculations and the energy corresponding to the absolute minimum of the (Q_{20}, Q_{30}) MFPES, is rather small (188, 266, and 70 keV for $^{198-202}$Dy, respectively).

The MFPESs shown in Fig. 1 also become softer along the octupole direction as one approaches ^{154}Dy, i.e., the neutron octupole magic number $N = 88$. In our calculations as well as in previous mac-mic ones [9], there is no static octupole deformation in this region. This is at variance with recent relativistic mean-field results [8] that predict octupole-deformed Dy isotopes with $N \approx 88$. However, for both $N \approx 88$ and $N \approx 134$ Dy isotopes, the softness displayed by the Gogny-D1M MFPESs along the Q_{30} direction (see also Fig. 4 of Ref. [8]) points towards the key role of dynamical beyond-mean-field correlations, i.e., symmetry restoration and/or quadrupole-octupole configuration mixing in the properties of the ground state and collective negative parity states in the studied nuclei. At this level, and at variance with Ref. [8], we conclude that the plain mean-field framework is not sufficient to extract conclusions about permanent octupole deformation effects in the considered nuclei. Therefore, we turn our attention to beyond-mean-field correlations in the next Sec. II B.

B. Dynamical beyond-mean-field correlations

In this section, we turn our attention to the impact of beyond-mean-field correlations in different low energy properties of the Dy isotopes considered. First, parity projection (after variation) calculations are discussed in Sec. II B 1. As shown, not only the MFPESs in Fig. 1, but also the parity projected potential energy surfaces obtained for some of the considered nuclei, exhibit a rather soft behavior along the octupole direction with a pronounced competition between reflection-symmetric and reflection-asymmetric configurations. As a result, not only symmetry restoration but also fluctuations in the collective coordinates should be considered for the studied nuclei. This is done in Sec. II B 2 within the framework of the symmetry-conserving 2D-GCM framework [11–14]. Since the octupole is the softest mode, the spatial reflection symmetry is the most important invariance to be restored. The simultaneous restoration of other symmetries, such as the rotational and particle number symmetries [22,23], is out of the scope of the present survey for technical reasons such as the large number of HO shells used and/or the number of degrees of freedom required in the 2D-GCM ansatz.

1. Parity symmetry restoration

Once the intrinsic HFB states $|\Phi(Q_{20}, Q_{30})\rangle$, discussed in the previous Sec. II A, are obtained the spatial reflection symmetry in each of those states is restored by means of parity projection after variation. In what follows, and for the sake of simplicity, we will use the notation $\mathbf{Q} = (Q_{20}, Q_{30})$ for the

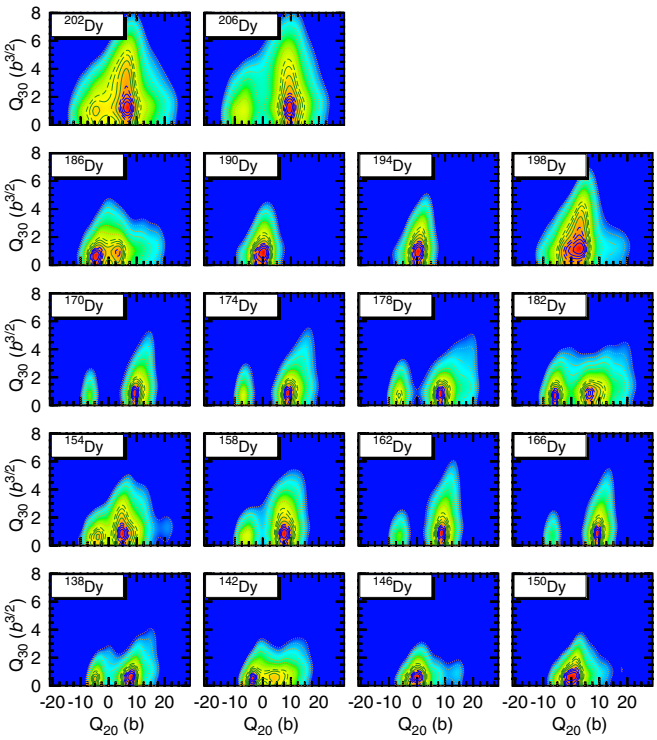

FIG. 3. Positive parity ($\pi = +1$) PPPESs computed with the Gogny-D1M EDF for a selected set of Dy isotopes. See nthe caption of Fig. 1 for the contour-line patterns and color scale.

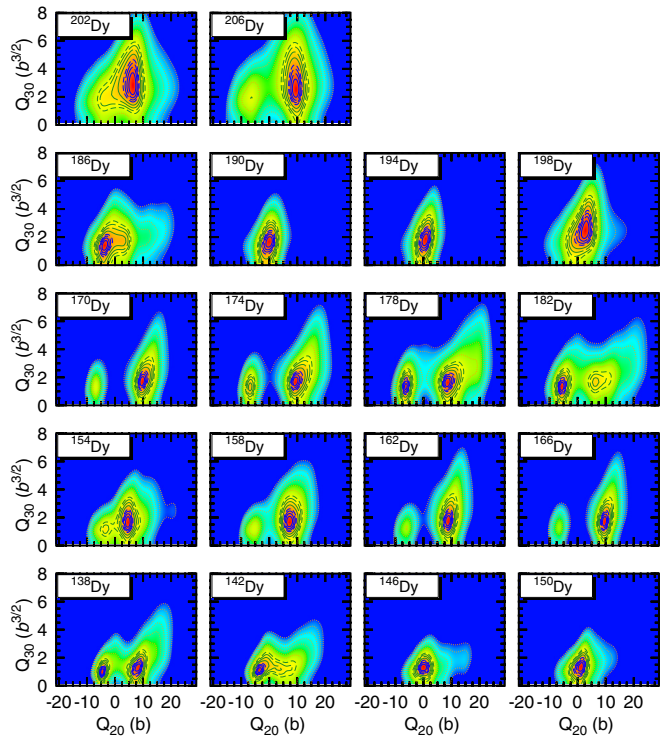

FIG. 4. Negative parity ($\pi = -1$) PPPESs computed with the Gogny-D1M EDF for a selected set of Dy isotopes. See the caption of Fig. 1 for the contour-line patterns and color scale.

pair of quadrupole and octupole deformation parameters that label each of the intrinsic HFB states, i.e., $|\Phi(Q_{20}, Q_{30})\rangle = |\Phi(\mathbf{Q})\rangle$. The projected states read

$$|\Phi^{\pi}(\mathbf{Q})\rangle = \hat{\mathcal{P}}^{\pi}|\Phi(\mathbf{Q})\rangle = \tfrac{1}{2}(1 + \pi\hat{\Pi})|\Phi(\mathbf{Q})\rangle, \qquad (9)$$

where the projection operator $\hat{\mathcal{P}}^{\pi}$ is written in terms of the desired parity quantum number $\pi = \pm 1$ and the parity operator $\hat{\Pi}$.

In the case of the density dependent Gogny-EDF, the projected energies

$$E_{\pi}(\mathbf{Q}) = \frac{\langle\Phi(\mathbf{Q})|\hat{H}\mathcal{P}^{\pi}|\Phi(\mathbf{Q})\rangle}{\langle\Phi(\mathbf{Q})|\mathcal{P}^{\pi}|\Phi(\mathbf{Q})\rangle} \qquad (10)$$

associated with the parity-projected states $|\Phi^{\pi}(\mathbf{Q})\rangle$ (9) have been computed using a mixed-density prescription in the density-dependent term of the EDF to avoid the pathologies found in the restoration of spatial symmetries [70–74]. We have also introduced first-order corrections in Eq. (10) to account for the fact that the parity-projected mean value of proton and neutron numbers usually differs from the nucleus's proton and neutron numbers [11,12,14]. The $\pi = +1$ and $\pi = -1$ parity-projected potential energy surfaces (PPPESs), depicted in Figs. 3 and 4 for a selected set of Dy isotopes as illustrative examples, are nothing else than the energies $E_{\pi}(\mathbf{Q})$, as functions of the quadrupole Q_{20} and octupole Q_{30} deformations of the intrinsic states. As in previous studies, in Fig. 4 we have omitted the $Q_{30} = 0$ line as the evaluation of $E_{\pi=-1}$ requires the nontrivial task of resolving numerically a zero over zero indeterminacy. Fortunately, the negative parity projected energy increases rapidly as the $Q_{30} = 0$ line is approached (see Fig. 5) and its limiting value [53] is high enough to not play a significant role in the discussion of the $\pi = -1$ PPPESs [11].

The comparison between the PPPESs and the MFPESs in Fig. 1, reveals that the quadrupole deformations corresponding to their absolute minima are close to each other. Moreover, from the comparison between the MFPESs and $\pi = +1$ PPPESs one realizes that, in spite of the changes in topography along the Q_{30} direction, the latter are also rather octupole soft and/or display a pronounced competition between reflection-symmetric and reflection-asymmetric configurations. This is illustrated in panels (a) and (b) of Fig. 5, where the $\pi = +1$ parity-projected energies obtained for ^{154}Dy and ^{202}Dy are plotted, as functions of Q_{30}, for fixed values of the quadrupole moment. At the HFB level, the ground state of ^{154}Dy is reflection symmetric whereas the one of ^{202}Dy shows a nonzero octupole moment. However, for both isotopes the $\pi = +1$ parity-projected curves in Fig. 5 display a minimum with a pocket around $Q_{30} = 1b^{3/2}$. In both cases, such an octupole-deformed minimum is less than 1.3 MeV deeper than the reflection-symmetric configuration, indicating that, in addition to parity symmetry restoration, fluctuations in the collective coordinates (in particular, the octupole coordinate which represents the softest mode) should be taken into account for the studied nuclei. On the other hand, the $\pi = -1$ PPPESs shown in Fig. 4 [see also panels (a) and (b) of Fig. 5] exhibit in all the cases absolute minima with

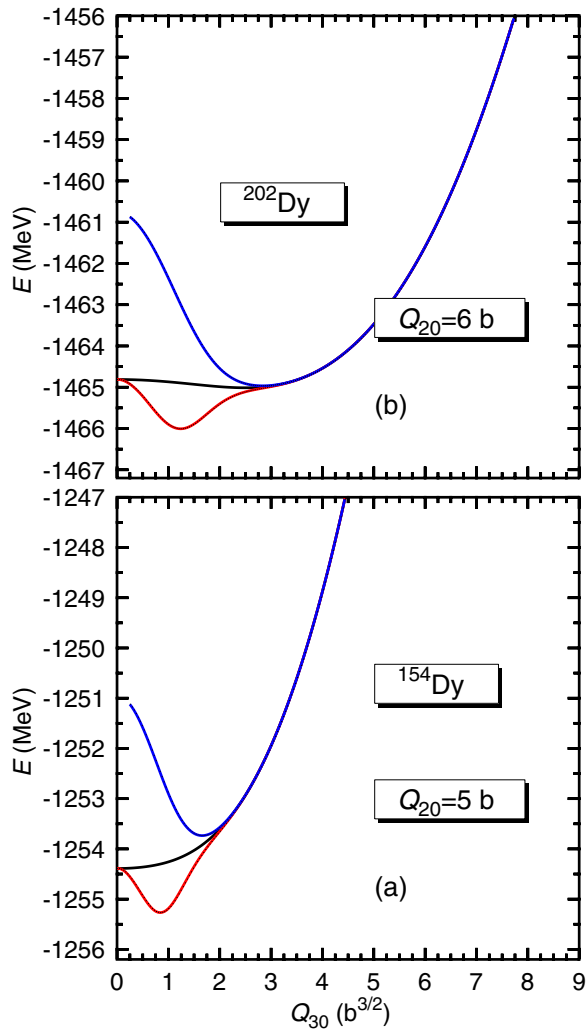

FIG. 5. The $\pi = +1$ (red) and $\pi = -1$ (blue) parity-projected energies are depicted as functions of the octupole moment Q_{30} for fixed values of the quadrupole moment Q_{20} in the nuclei ^{154}Dy and ^{202}Dy. The corresponding HFB energies (black) are also included in the plots. Results were obtained with the Gogny-D1M EDF.

octupole deformations larger than the ones in the MFPESs and $\pi = +1$ PPPESs.

2. *Symmetry-conserving 2D-GCM quadrupole-octupole configuration mixing*

The results discussed in Secs. II A and II B 1 indicate that not only parity symmetry restoration but also symmetry-projected quadrupole-octupole configuration mixing is required to disentangle the stability of octupole deformation effects in the studied Dy isotopes. To this end, we consider the following 2D-GCM superposition of HFB states $|\Phi(\mathbf{Q})\rangle$:

$$\left|\Psi^{\pi}_{\sigma}\right\rangle = \int_{\mathcal{D}} d\mathbf{Q} f^{\pi}_{\sigma}(\mathbf{Q})|\Phi(\mathbf{Q})\rangle, \tag{11}$$

where both positive and negative octupole moments are included in the integration domain $\mathcal{D}$. The 2D-GCM ansatz $|\Psi^{\pi}_{\sigma}\rangle$ accounts for both reflection symmetry restoration and (Q_{20}, Q_{30}) fluctuations [11–14]. In Eq. (11) $\pi = \pm 1$ represents the parity quantum number, while the index σ numbers the different GCM solutions.

The amplitudes $f^{\pi}_{\sigma}(\mathbf{Q})$ should be determined dynamically via the solution of the corresponding Griffin-Hill-Wheeler (GHW) equation [1,11,12,14], written in terms of nondiagonal norm $\mathcal{N}(\mathbf{Q}, \mathbf{Q}') = \langle\Phi(\mathbf{Q})|\Phi(\mathbf{Q}')\rangle$ and Hamiltonian $\mathcal{H}(\mathbf{Q}, \mathbf{Q}') = \langle\Phi(\mathbf{Q})|\hat{H}|\Phi(\mathbf{Q}')\rangle$ overlaps. In the evaluation of the Hamiltonian overlap one has to pay special attention to avoid the use of nonequivalent bases in the left and right HFB states [75]. In our case, this is accomplished by using the same oscillator lengths for all HFB states considered in the GCM mixing [76,77]. For the evaluation of the density-dependent contribution of the Gogny-EDF to the Hamiltonian overlap we considered a mixed-density prescription in the density-dependent term of the EDF [11,12,14,74]. Finally, perturbative first-order corrections in the mean value of both proton and neutron numbers have been considered [11,12,14,74].

The solution of the GHW equation provides the dynamical amplitudes $f^{\pi}_{\sigma}(\mathbf{Q})$. Nevertheless, in the case of a nonorthogonal basis of HFB states $|\Phi(\mathbf{Q})\rangle$, i.e., $\langle\Phi(\mathbf{Q})|\Phi(\mathbf{Q}')\rangle \neq \delta(\mathbf{Q} - \mathbf{Q}')$, such amplitudes $f^{\pi}_{\sigma}(\mathbf{Q})$ cannot be assigned a quantum mechanical probabilistic interpretation [1]. One then introduces the collective wave functions [1,11,74]

$$G^{\pi}_{\sigma}(\mathbf{Q}) = \int d\mathbf{Q}' \mathcal{N}^{\frac{1}{2}}(\mathbf{Q}, \mathbf{Q}') f^{\pi}_{\sigma}(\mathbf{Q}') \tag{12}$$

written in terms of the amplitudes $f^{\pi}_{\sigma}(\mathbf{Q})$, Eq. (11), and the operational square root $\mathcal{N}^{\frac{1}{2}}(\mathbf{Q}, \mathbf{Q}')$ of the norm overlap kernel [1,74].

The reduced transition probabilities $B(E1, 1^- \to 0^+)$ and $B(E3, 3^- \to 0^+)$ were computed using the rotational model approximation for $K = 0$ bands

$$B(E\lambda, \lambda^- \to 0^+) = \frac{e^2}{4\pi}\left|\left\langle\Psi^{\pi=-1}_{\sigma}\middle|\hat{\mathcal{O}}_{\lambda}\middle|\Psi^{\pi=+1}_{\sigma=1}\right\rangle\right|^2, \tag{13}$$

where σ corresponds to the first 2D-GCM excited negative-parity state. The electromagnetic transition operators $\hat{\mathcal{O}}_1$ and $\hat{\mathcal{O}}_3$ represent the dipole moment operator and the proton component $\hat{Q}_{30,\text{prot}}$ of the octupole operator, respectively. The overlaps $\langle\Psi^{\pi}_{\sigma}|\hat{\mathcal{O}}_{\lambda}|\Psi^{\pi'}_{\sigma'}\rangle$ have been evaluated using the expressions given in Ref. [11].

The collective wave functions (12) corresponding to the ground and lowest negative-parity states of the nuclei ^{198}Dy, ^{202}Dy, and ^{206}Dy are depicted in Fig. 6, as illustrative examples. Similar results were obtained for other Dy isotopes. Note that at the HFB level ^{198}Dy and ^{202}Dy (^{206}Dy) exhibit reflection-asymmetric (reflection-symmetric) ground states.

The values obtained for the average quadrupole moments

$$(\bar{Q}_{20})^{\pi}_{\sigma} = \left\langle\Psi^{\pi}_{\sigma}\middle|\hat{Q}_{20}\middle|\Psi^{\pi}_{\sigma}\right\rangle, \tag{14}$$

corresponding to the 2D-GCM ground states $(\bar{Q}_{20})^{\pi=+1}_{\sigma=1}$, display a pattern similar to the one obtained at the mean-field level [see panel (a) of Fig. 2]. The pattern followed by $(\bar{Q}_{20})^{\pi=+1}_{\sigma=1}$, as well as the one followed by the average quadrupole moments corresponding to the first negative-parity states $(\bar{Q}_{20})^{\pi=-1}_{\sigma}$, clearly reflect the impact of the neutron

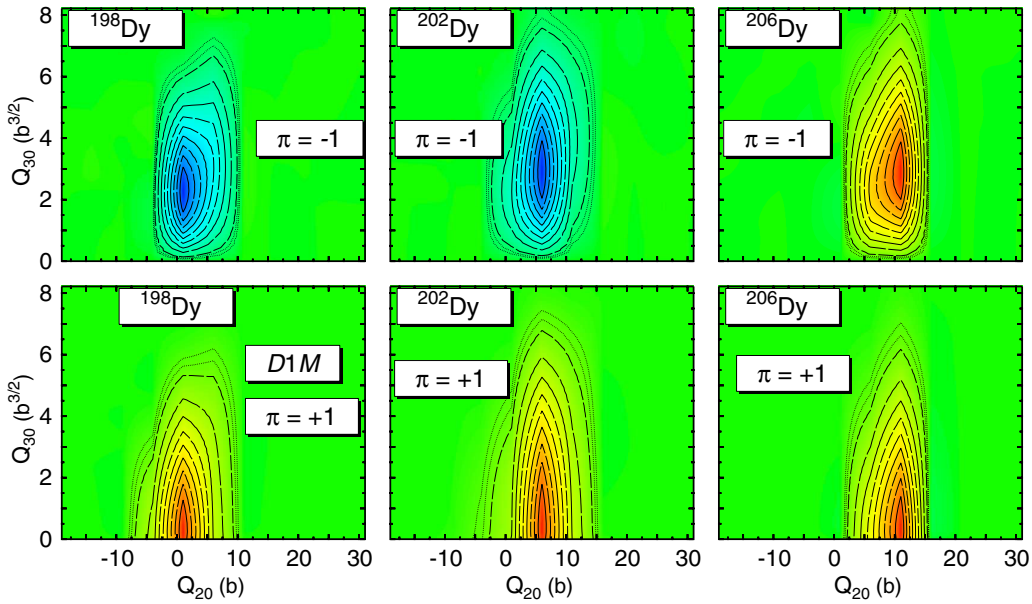

FIG. 6. Collective wave functions (12) corresponding to the ground (bottom panels) and lowest negative-parity (top panels) states of the nuclei ^{198}Dy, ^{202}Dy, and ^{206}Dy. The succession of solid, long-dashed, and short-dashed contour lines starts at 90% of the maximum value up to 10% of it. The two dotted-line contours correspond to the tail of the amplitude (5% and 1% of the maximum value). The color scale ranges from red (maximum value) to green (zero). Results have been obtained with the Gogny-D1M EDF. For more details, see the main text.

shell closures $N = 82$ and $N = 126$ in the evolution of the quadrupole properties along the considered isotopic chain.

The ground state collective wave functions $G^{\pi=+1}_{\sigma=1}(\mathbf{Q})$, shown in the bottom panels of Fig. 6 for the $N \approx 134$ isotopes ^{198}Dy, ^{202}Dy, and ^{206}Dy exhibit a large spreading along the Q_{30} direction. This is also the case for the $G^{\pi=+1}_{\sigma=1}(\mathbf{Q})$ amplitudes corresponding to $N \approx 88$ Dy isotopes. This reflects the octupole-soft character of the Gogny-D1M 2D-GCM ground states in the case of $N \approx 88$ and $N \approx 134$ Dy isotopes. However, for all the nuclei studied in this paper, the $G^{\pi=+1}_{\sigma=1}(\mathbf{Q})$ amplitudes exhibit peaks around $Q_{30} = 0$ pointing to an octupole-vibrational character.

In order to access dynamical octupole deformation effects at a more quantitative level, we computed the average octupole moment [11,12,14]

$$(\bar{Q}_{30})^{\pi}_{\sigma} = 4 \int_{\mathcal{D}} d\mathbf{Q} d\mathbf{Q}' G^{\pi\,*}_{\sigma}(\mathbf{Q}) \mathcal{Q}_{30}(\mathbf{Q}, \mathbf{Q}') G^{\pi}_{\sigma}(\mathbf{Q}') \qquad (15)$$

and obtained that, for all the considered nuclei, the ground state $(\bar{Q}_{30})^{\pi=+1}_{\sigma=1}$ values are within the range $0.25b^{3/2} \leqslant (\bar{Q}_{30})^{\pi=+1}_{\sigma=1} \leqslant 0.93b^{3/2}$. On the one hand, this indicates an enhanced octupolarity in their ground states via dynamical zero-point 2D-GCM quantum fluctuations. On the other hand, even the largest $(\bar{Q}_{30})^{\pi=+1}_{\sigma=1}$ values obtained for $N \approx 134$ isotopes are less than half of the (static) HFB ground state octupole deformations. Thus, to a large extent, even the static octupole deformation effects predicted at the Gogny-HFB level around $N = 134$ are washed out once symmetry-conserving quadrupole-octupole configuration mixing is taken into account.

The previous results point towards octupole-vibrational features in the Dy chain, and raise questions about the conclusions extracted in Ref. [8] from the results of a plain mean-field calculation. In this reference the existence of permanent octupole deformations in $N = 88$ and $N = 134$ Dy isotopes is concluded. Let us stress that results (not shown) similar to the ones already discussed have also been obtained in the present study with other parametrizations of the Gogny EDF, such as D1S [10] and D1M* [67] (see also the discussion below).

The collective wave functions $G^{\pi=-1}_{\sigma}(\mathbf{Q})$ corresponding to the lowest negative-parity states of the nuclei ^{198}Dy, ^{202}Dy, and ^{206}Dy, shown in the top panels of Fig. 6 are odd under the exchange $Q_{30} \to -Q_{30}$. They reach a zero value at $Q_{30} = 0$ as well as a maximum and a minimum, one for a positive octupole deformation and the other at the corresponding negative value. As a result, the amplitudes $G^{\pi=-1}_{\sigma}(\mathbf{Q})$ in Fig. 6 always display a maximum or a minimum for $Q_{30} \neq 0$. For each of the studied isotopes, the $(\bar{Q}_{30})^{\pi=-1}_{\sigma=}$ value is close to the octupole deformation corresponding to the minimum of the $\pi = -1$ PPPESs (see Fig. 4).

The 2D-GCM excitation energies $\Delta E_{\text{neg-par}}$ of the first negative-parity states as well as the reduced transitions probabilities $B(E1)$ and $B(E3)$ obtained for the considered Dy isotopes, are plotted in panels (a)–(c) of Fig. 7, as functions of the neutron number. Additional results for the parametrizations D1S and D1M* are also included in the figure. As can be seen, with minor exceptions, the results obtained with different parametrizations are rather similar. This points towards the robustness of the predicted trends with respect to the underlying Gogny-EDF.

As functions of the neutron number, the 2D-GCM energies $\Delta E_{\text{neg-par}}$ display two pronounced minima, one at $N = 88$ and the other at $N = 134$. These Gogny 2D-GCM results indicate that, at a dynamical beyond-mean-field level, both $N = 88$ and $N = 134$ represent (on average) octupole magic

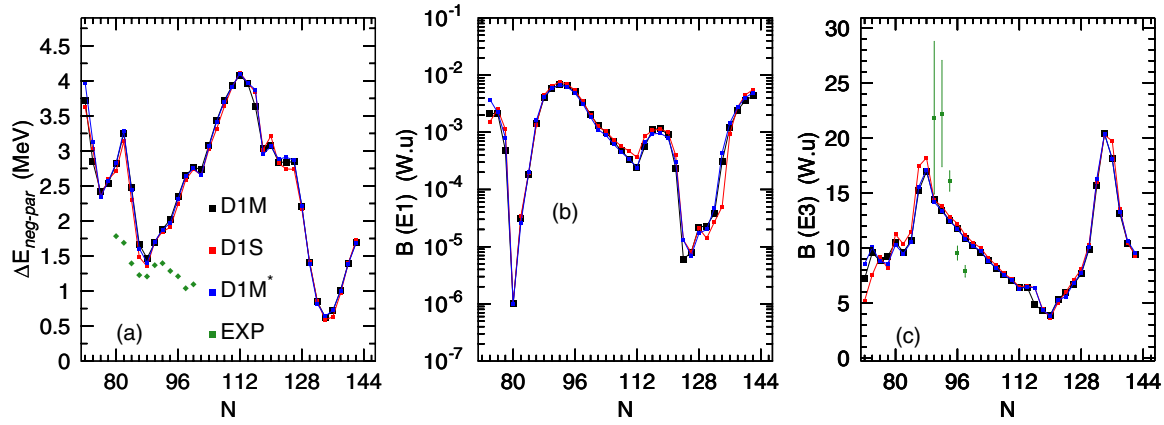

FIG. 7. The 2D-GCM excitation energies of the first negative-parity states [panel (a)], the reduced transitions probabilities $B(E1)$ [panel (b)] and $B(E3)$ [panel (c)] are plotted for $^{138-208}$Dy as functions of the neutron number. Results were obtained with the parametrizations D1M, D1S, and D1M* of the Gogny-EDF. Experimental data were taken from Ref. [68]. For more details, see the main text.

numbers along the studied isotopic chain. We stress that no static octupole deformation is obtained for $N \approx 88$ isotopes at the mean-field level. Moreover, the ground state collective wave functions for those isotopes are peaked around $Q_{30} = 0$. These results suggest that, in the case of Dy isotopes, the octupole collectivity around $N = 88$ is more vibrational-like in character than suggested in Ref. [8] on the base of plain mean-field calculations. Static octupole deformations have been obtained at the Gogny-HFB level for $N \approx 134$ isotopes. However, as already mentioned, their ground state collective wave functions are also peaked around $Q_{30} = 0$, while the corresponding mean-field deformation effects are reduced to more than half once 2D-GCM zero-point fluctuations are included. This suggests that the prominent minimum observed in panel (a) of the figure at $N = 134$ should also be associated with a vibrational character of the excitation instead of permanent octupole deformation effects. Regarding the comparison with the still scarce data [68], the predicted $\Delta E_{\text{neg-par}}$ values reproduce reasonably well the experimental trend in the immediate neighborhood of $N = 88$, while they overestimate considerably the available experimental values as one moves away from this neutron number.

The $B(E1)$ strengths shown in panel (b) of the same figure exhibit two minima, one at $N \approx 82$ and the other at $N \approx 126$. From a dynamical point of view, it is precisely around these neutron numbers where the overlap $\langle \Psi_\sigma^{\pi=-1} | \hat{\mathcal{O}}_1 | \Psi_{\sigma=1}^{\pi=+1} \rangle$ (with $\hat{\mathcal{O}}_1$ being the dipole moment operator) reaches its minimum. Here, one should keep in mind that the behavior of the $B(E1)$ strengths is not directly related to the one observed in the $\Delta E_{\text{neg-par}}$ energies and/or the $B(E3)$ reduced transition probabilities (see below). In fact, via the strong dependence of the dipole moment on the underlying single-particle structure, the $B(E1)$ values might display strong suppression for some specific neutron numbers [11–14,53], specially around neutron shell closures.

The trend observed in the predicted $B(E3)$ values correlates well with the one in the $\Delta E_{\text{neg-par}}$ energies, i.e., as functions of the neutron number the $B(E3)$ strengths exhibit two pronounced maxima at $N = 88$ and $N = 134$ where the $\Delta E_{\text{neg-par}}$ energies display two pronounced minima. The comparison with the available experimental data [68] reveals that, in spite of the quantitative differences, the predicted $E3$ trend reproduces the increased octupole collectivity around $N = 88$ as well as its sudden decrease with increasing neutron number. We stress that the $E3$ collectivity around $N = 88$ and $N = 134$ is not the result of permanent mean-field octupolarity around those neutron numbers, as concluded in Ref. [8], but directly reflects the key role played by dynamical fluctuations. In fact, via the structure of the corresponding collective wave functions, the 2D-GCM overlap $\langle \Psi_\sigma^{\pi=-1} | \hat{\mathcal{O}}_3 | \Psi_{\sigma=1}^{\pi=+1} \rangle$ (with $\hat{\mathcal{O}}_3$ being the proton component of the octupole operator) reflects the difference $|(\bar{Q}_{30})_{\sigma=1}^{\pi=+1} - (\bar{Q}_{30})_\sigma^{\pi=-1}|$ between the dynamical ground $(\bar{Q}_{30})_{\sigma=1}^{\pi=+1}$ and first negative-parity $(\bar{Q}_{30})_\sigma^{\pi=-1}$ state deformations, i.e., the larger (smaller) the difference, the smaller (larger) the overlap $\langle \Psi_\sigma^{\pi=-1} | \hat{\mathcal{O}}_3 | \Psi_{\sigma=1}^{\pi=+1} \rangle$. It is precisely the more pronounced (dynamical) enhancement of ground state octupolarity [i.e., larger $(\bar{Q}_{30})_{\sigma=1}^{\pi=+1}$ values] obtained as one approaches both $N = 88$ and $N = 134$ that leads to a reduction of the difference $|(\bar{Q}_{30})_{\sigma=1}^{\pi=+1} - (\bar{Q}_{30})_\sigma^{\pi=-1}|$ and, therefore, to larger $B(E3)$ strengths as compared with the ones obtained as we move away from these two neutron octupole magic numbers.

III. SUMMARY AND CONCLUSIONS

In this paper we have carried out calculations, at both the mean-field level and beyond, to address the emergence and stability of (static) mean-field octupole deformation effects in Dy isotopes from drip line to drip line. To this end, we have resorted to the models already employed in Refs. [11–14] in other regions of the nuclear chart.

Contrary to recent reflection-asymmetric relativistic mean field results [8] but in agreement with previous macmic [9] results, at the Gogny-HFB level static octupole deformations have been found only for $N \approx 134$ isotopes, while nuclei with $N \approx 88$ exhibit reflection-symmetric ground states. Moreover, even in the case of nuclei with octupole deformed Gogny-D1M mean-field ground states

(i.e., $^{198-202}$Dy), the HFB octupole correlation energies Eq. (8) are always smaller than 300 keV. This, as well as the octupole softness of the corresponding MFPESs, indicate that the plain mean-field framework is not sufficient to extract conclusions about permanent octupole deformation effects in Dy isotopes.

The results obtained in this paper, together with previous studies of the octupole dynamics in other regions of the nuclear chart [11–14,64,65], represent a warning to the use of the mean-field approach to extract conclusions on the permanent and/or vibrational nature of octupolarity in atomic nuclei with shallow octupole minima and/or octupole-soft MFPESs. Furthermore, it has been shown that the octupole-softness found in the MFPESs, especially around the neutron numbers $N = 88$ and $N = 134$, also extends to the parity-projected potential energy surfaces, pointing towards the key role of 2D-GCM symmetry-conserving configuration mixing in the studied nuclei.

At the 2D-GCM level, zero-point quantum fluctuations associated with the restoration of reflection symmetry and fluctuations in the collective (Q_{20}, Q_{30}) coordinates, lead to an enhanced octupolarity for all the considered isotopes, albeit with dynamical deformations less than half of the largest values obtained at the mean-field level. Therefore, to a large extent, the (static) mean-field octupole deformation effects are washed out in Dy nuclei once 2D-GCM fluctuations are taken into account. Our analysis of the 2D-GCM collective wave functions as well as the trends of the predicted $\Delta E_{\text{neg-par}}$ excitation energies and $B(E3)$ strengths, corroborate an increased octupole collectivity in Dy isotopes with $N \approx 88$ and $N \approx 134$. However, we stress that such increased octupolarity is a (dynamical) vibrational-like effect that is not directly related to permanent mean-field octupole deformation in the considered nuclei.

The predicted $\Delta E_{\text{neg-par}}$ values reproduce reasonably well the available experimental data in the immediate neighborhood of $N = 88$, while in the $B(E3)$ case the calculations account qualitatively for the increased octupole collectivity around $N = 88$ as well as its sudden decrease with increasing neutron number. The predicted $B(E1)$ reduced transition probabilities display strong suppression around $N \approx 82$ and $N \approx 126$. Furthermore, the D1S, D1M*, and D1M parameter sets provide rather similar results, pointing towards the robustness of the predicted trends with respect to the underlying Gogny EDF.

ACKNOWLEDGMENTS

The work of R.R.-G. was supported within the framework of the (distinguished researcher) María Zambrano Program, Ministry of Universities and Seville University, Spain. The work of L.M.R. was supported by Spanish Agencia Estatal de Investigacion (AEI) of the Ministry of Science and Innovation under Grant No. PID2021-127890NB-I00.

[1] P. Ring and P. Schuck, *The Nuclear Many-Body Problem* (Springer, Berlin, 1980).
[2] P. A. Butler and W. Nazarewicz, Rev. Mod. Phys. **68**, 349 (1996).
[3] S. N. T. Majola *et al.*, Phys. Rev. C **100**, 034322 (2019).
[4] T. Lauritsen, R. V. F. Janssens, M. P. Carpenter, P. Fallon *et al.*, Phys. Rev. Lett. **89**, 282501 (2002).
[5] G. L. Zimba, J. F. Sharpey-Schafer, P. Jones, S. P. Bvumbi *et al.*, Phys. Rev. C **94**, 054303 (2016).
[6] D. J. Hartley *et al.*, Phys. Rev. C **95**, 014321 (2017).
[7] A. Aprahamian, X. Wu, S. R. Lesher, D. D. Warner *et al.*, Nucl. Phys. A **764**, 42 (2006).
[8] Yu.-T. Qiu, X.-W. Wang, and J.-Y. Guo, Phys. Rev. C **106**, 034301 (2022).
[9] P. Möller, A. J. Sierk, T. Ichikawa, and H. Sagawa, At. Data Nucl. Data Tables **109–110**, 1 (2016).
[10] J. F. Berger, M. Girod, and D. Gogny, Nucl. Phys. A **428**, 23 (1984).
[11] R. Rodríguez-Guzmán, L. M. Robledo, and P. Sarriguren, Phys. Rev. C **86**, 034336 (2012).
[12] R. Rodríguez-Guzmán, Y. M. Humadi, and L. M. Robledo, J. Phys. G: Nucl. Part. Phys. **48**, 015103 (2021).
[13] L. M. Robledo and P. A. Butler, Phys. Rev. C **88**, 051302(R) (2013).
[14] R. Rodríguez-Guzmán and L. M. Robledo, Phys. Rev. C **103**, 044301 (2021).
[15] I. Ahmad and P. A. Butler, Ann. Rev. Nucl. Part. Sci. **43**, 71 (1993).
[16] P. A. Butler, J. Phys. G **43**, 073002 (2016).
[17] P. A. Butler and L. Willmann, Nucl. Phys. News **25**, 12 (2015).
[18] S. K. Tandel, M. Hemalatha, A. Y. Deo, S. B. Patel, R. Palit, T. Trivedi, J. Sethi, S. Saha, D. C. Biswas, and S. Mukhopadhyay, Phys. Rev. C **87**, 034319 (2013).
[19] H. J. Li, S. J. Zhu, J. H. Hamilton, E. H. Wang, A. V. Ramayya, Y. J. Chen, J. K. Hwang, J. Ranger, S. H. Liu, Z. G. Xiao, Y. Huang, Z. Zhang, Y. X. Luo, J. O. Rasmussen, I. Y. Lee, G. M. Ter-Akopian, Y. T. Oganessian, and W. C. Ma, Phys. Rev. C **90**, 047303 (2014).
[20] I. Ahmad, R. R. Chasman, J. P. Greene, F. G. Kondev, and S. Zhu, Phys. Rev. C **92**, 024313 (2015).
[21] B. Bucher, S. Zhu, C. Y. Wu, R. V. F. Janssens, D. Cline, A. B. Hayes *et al.*, Phys. Rev. Lett. **116**, 112503 (2016).
[22] B. Bucher, S. Zhu, C. Y. Wu, R. V. F. Janssens, R. N. Bernard, L. M. Robledo *et al.*, Phys. Rev. Lett. **118**, 152504 (2017).
[23] R. N. Bernard, L. M. Robledo, and T. R. Rodriguez, Phys. Rev. C **93**, 061302(R) (2016).
[24] P. A. Butler, L. P. Gaffney, P. Spagnoletti, K. Abrahams, M. Bowry, J. Cederkall *et al.*, Phys. Rev. Lett. **124**, 042503 (2020).
[25] L. P. Gaffney *et al.*, Nature (London) **497**, 199 (2013).
[26] P. A. Butler *et al.*, Nat. Commun. **10**, 2473 (2019).
[27] M. M. R. Chishti, D. OD'onnell, G. Battaglia, M. Bowry, D. A. Jaroszynski, B. S. N. Singh, M. Scheck, P. Spagnoletti, and J. F. Smith, Nat. Phys. **16**, 853 (2020).
[28] R. Rodríguez-Guzmán and L. M. Robledo, Phys. Rev. C **89**, 054310 (2014).
[29] R. Rodríguez-Guzmán and L. M. Robledo, Eur. Phys. J. A **53**, 245 (2017).
[30] R. Rodríguez-Guzmán, Y. M. Humadi, and L. M. Robledo, Eur. Phys. J. A **56**, 43 (2020).

[31] N. Schunck and L. M. Robledo, Rep. Prog. Phys. **79**, 116301 (2016).
[32] M. Warda and L. M. Robledo, Phys. Rev. C **84**, 044608 (2011).
[33] P. Möller and J. R. Nix, Nucl. Phys. A **361**, 117 (1981).
[34] A. Gyurkovich, A. Sobiczewski, B. Nerlo-Pomorska, and K. Pomorski, Phys. Lett. B **105**, 95 (1981).
[35] W. Nazarewicz, P. Olanders, I. Ragnarsson, J. Dudek, G. Leander, P. Möller, and E. Ruchowska, Nucl. Phys. A **429**, 269 (1984).
[36] P. Möller, J. Nix, W. D. Meyers, and W. Swiatecki, At. Data Nucl. Data Tables **59**, 185 (1995).
[37] P. Möller, R. Bengtson, B. G. Carlsson, P. Olivius, T. Ichikawa, H. Sagawa, and A. Iwamoto, At. Data Nucl. Data Tables **94**, 758 (2008).
[38] K. Nomura, D. Vretenar, T. Niksic, and B.-N. Lu, Phys. Rev. C **89**, 024312 (2014).
[39] K. Nomura, T. Niksic, and D. Vretenar, Phys. Rev. C **97**, 024317 (2018).
[40] K. Nomura, D. Vretenar, and B.-N. Lu, Phys. Rev. C **88**, 021303(R) (2013).
[41] K. Nomura, R. Rodríguez-Guzmán, and L. M. Robledo, Phys. Rev. C **92**, 014312 (2015).
[42] K. Nomura, R. Rodríguez-Guzmán, Y. M. Humadi, L. M. Robledo, and J. E. García-Ramos, Phys. Rev. C **102**, 064326 (2020).
[43] K. Nomura, R. Rodríguez-Guzmán, L. M. Robledo, and J. E. García-Ramos, Phys. Rev. C **103**, 044311 (2021).
[44] K. Nomura, R. Rodríguez-Guzmán, L. M. Robledo, J. E. García-Ramos, and N. C. Hernández, Phys. Rev. C **104**, 044324 (2021).
[45] K. Nomura, R. Rodríguez-Guzmán, and L. M. Robledo, Phys. Rev. C **104**, 054320 (2021).
[46] S. Marcos, H. Flocard, and P. H. Heenen, Nucl. Phys. A **410**, 125 (1983).
[47] P. Bonche, P.-H. Heenen, H. Flocard, and D. Vautherin, Phys. Lett. B **175**, 387 (1986).
[48] P. Bonche, S. J. Krieger, M. S. Weiss, J. Dobaczewski, H. Flocard, and P.-H. Heenen, Phys. Rev. Lett. **66**, 876 (1991).
[49] P.-H. Heenen, J. Skalski, P. Bonche, and H. Flocard, Phys. Rev. C **50**, 802 (1994).
[50] J. Erler, K. Langanke, H. P. Loens, G. Martínez-Pinedo, and P.-G. Reinhard, Phys. Rev. C **85**, 025802 (2012).
[51] L. M. Robledo, J. L. Egido, J. F. Berger, and M. Girod, Phys. Lett. B **187**, 223 (1987).
[52] L. M. Robledo, J. L. Egido, B. Nerlo-Pomorska, and K. Pomorski, Phys. Lett. B **201**, 409 (1988).
[53] J. L. Egido and L. M. Robledo, Nucl. Phys. A **518**, 475 (1990); **524**, 65 (1991); **545**, 589 (1992).
[54] E. Garrote, J. L. Egido, and L. M. Robledo, Phys. Rev. Lett. **80**, 4398 (1998); Nucl. Phys. A **654**, 723c (1999).
[55] L. M. Robledo, M. Baldo, P. Schuck, and X. Viñas, Phys. Rev. C **81**, 034315 (2010).
[56] W. H. Long, J. Meng, N. Van Giai, and S. G. Zhou, Phys. Rev. C **69**, 034319 (2004).
[57] Z. P. Li, B. Y. Song, J. M. Yao, D. Vretenar, and J. Meng, Phys. Lett. B **726**, 866 (2013).
[58] L. M. Robledo and R. Rodríguez-Guzmán, J. Phys. G: Nucl. Part. Phys. **39**, 105103 (2012).
[59] S. Ebata and T. Nakatsukasa, Phys. Scr. **92**, 064005 (2017).
[60] S. Y. Xia, H. Tao, Y. Lu, Z. P. Li, T. Niksic, and D. Vretenar, Phys. Rev. C **96**, 054303 (2017).
[61] S. E. Agbemava, A. V. Afanasjev, and P. Ring, Phys. Rev. C **93**, 044304 (2016).
[62] S. E. Agbemava and A. V. Afanasjev, Phys. Rev. C **96**, 024301 (2017).
[63] Y. Cao, S. E. Agbemava, A. V. Afanasjev, W. Nazarewicz, and E. Olsen, Phys. Rev. C **102**, 024311 (2020).
[64] L. M. Robledo and G. F. Bertsch, Phys. Rev. C **84**, 054302 (2011).
[65] L. M. Robledo, J. Phys. G: Nucl. Part. Phys. **42**, 055109 (2015).
[66] S. Goriely, S. Hilaire, M. Girod, and S. Péru, Phys. Rev. Lett. **102**, 242501 (2009).
[67] C. Gonzalez-Boquera, M. Centelles, X. Vinas, and L. M. Robledo, Phys. Lett. B **779**, 195 (2018).
[68] T. Kibédi and R. H. Spear, At. Data Nucl. Data Tables **80**, 35 (2002).
[69] L. M. Robledo and G. F. Bertsch, Phys. Rev. C **84**, 014312 (2011).
[70] R. R. Rodríguez-Guzmán, J. L. Egido, and L. M. Robledo, Nucl. Phys. A **709**, 201 (2002)
[71] J. L Egido and L. M. Robledo, in *Extended Density Functionals in Nuclear Structure Physics*, Lecture Notes in Physics Vol. 641 (Springer, Berlin, 2004), p. 269.
[72] L. M. Robledo, Int. J. Mod. Phys. E **16**, 337 (2007).
[73] L. M. Robledo, J. Phys. G: Nucl. Part. Phys. **37**, 064020 (2010).
[74] J. A. Sheikh, J. Dobaczewski, P. Ring, L. M. Robledo, and C. Yannouleas, J. Phys. G: Nucl. Part. Phys. **48**, 123001 (2021).
[75] L. M. Robledo, Phys. Rev. C **50**, 2874 (1994).
[76] L. M. Robledo, Phys. Rev. C **105**, L021307 (2022).
[77] L. M. Robledo, Phys. Rev. C **105**, 044317 (2022).